Meteoritics & Planetary Science 42, Nr 10, 1751–1762 (2007)
Abstract available online at http://meteoritics.org

Characterization of the lithological contact in the shergottite EETA79001—A record of igneous differentiation processes on Mars

Deon VAN NIEKERK[1*], Cyrena Anne GOODRICH[2], G. Jeffrey TAYLOR[1], and Klaus KEIL[1]

[1]Hawai'i Institute of Geophysics and Planetology, School of Ocean and Earth Science and Technology, University of Hawai'i, Manoa, Honolulu, Hawai'i 96822, USA
[2]Department of Physical Sciences, Kingsborough Community College, Brooklyn, New York 11235, USA
[*]Corresponding author. E-mail: dionysos@higp.hawaii.edu

(Received 11 December 2005; revision accepted 29 April 2007)

Abstract–Elephant Moraine (EET) A79001 is the only Martian meteorite that consists of both an olivine-phyric shergottite (lithology A) and a basaltic shergottite (lithology B). The presence of these lithologies in one rock has previously been ascribed to mixing processes (either magmatic or impact-induced). Here we present data regarding phase changes across the contact between the lithologies. These data show that the contact is gradational and suggest that it is a primary igneous feature consistent with crystallization of a single cooling magma. We present a model to establish a petrogenetic connection between an olivine-phyric and a basaltic shergottite through differentiation.

The model involves the shallow or surface emplacement of a magma that contained pre-eruptive solids (phenocrysts and minor xenocrysts). Subsequent differentiation via crystal settling and in situ crystallization (Langmuir 1989) resulted in a layered sequence of lithology A overlain by lithology B, with gradations in modal abundance of maskelynite (increasing from A to B) and pigeonite/maskelynite (decreasing from A to B), and a gradational change in pattern of pyroxene zonation (zones of magnesian augite separating magnesian and ferroan pigeonite appear and thicken into B) across the contact. A pigeonite phenocryst-bearing zone near the contact in lithology B appears to be intermediate between lithology A and the bulk of lithology B (which resembles basaltic shergottite Queen Alexandra Range [QUE] 94201). Re-examination of Sr isotopic compositions in lithology A and across the contact is required to test and constrain the model.

INTRODUCTION

The shergottite-nakhlite-chassignite (SNC) meteorites are thought to come from Mars (e.g., Treiman et al. 2000). They consist of basalts, lherzolites, clinopyroxenites, dunites, and an orthopyroxenite. The shergottites comprise basaltic shergottites, olivine-phyric shergottites, and lherzolitic shergottites—all of which share some compositional characteristics. For almost 20 years, lithology A of Elephant Moraine (EET) A79001 was the only known olivine-phyric shergottite. A recent series of finds, however, have led to the recognition of olivine-phyric shergottites as a distinct group of the shergottite family (Goodrich 2002). The olivine-phyric shergottites, like the basaltic shergottites, consist of pigeonite, augite, and maskelynite (shocked plagioclase) with minor spinel and phosphates. They also contain phenocrysts of olivine, and chemically resemble terrestrial picrites. Lherzolitic shergottites are cumulates that are dominated by olivine and pigeonite with interstitial maskelynite and some spinel (Goodrich 2002; McSween and Treiman 1998).

EETA79001 is a shergottite that contains two dominant lithologies: lithology A, which is olivine-phyric, and lithology B, which is basaltic (e.g., Meyer 2003). Models for the petrogenesis of EETA79001 have largely focused on the interpretation that lithology A is a mixture of a basaltic shergottite-like magma (represented by lithology B) and ultramafic (possibly lherzolitic shergottite-like) material. The mechanism of mixing has been variously suggested to be assimilation of xenolithic material (McSween and Jarosewich 1983), magma mixing (Wadhwa et al. 1994), or impact mixing (Mittlefehldt et al. 1999). In contrast, Goodrich (2003) argued that the majority of material in lithology A formed by continuous crystallization of a single magma, with loss of a late, fractionated liquid that might be represented by lithology B.

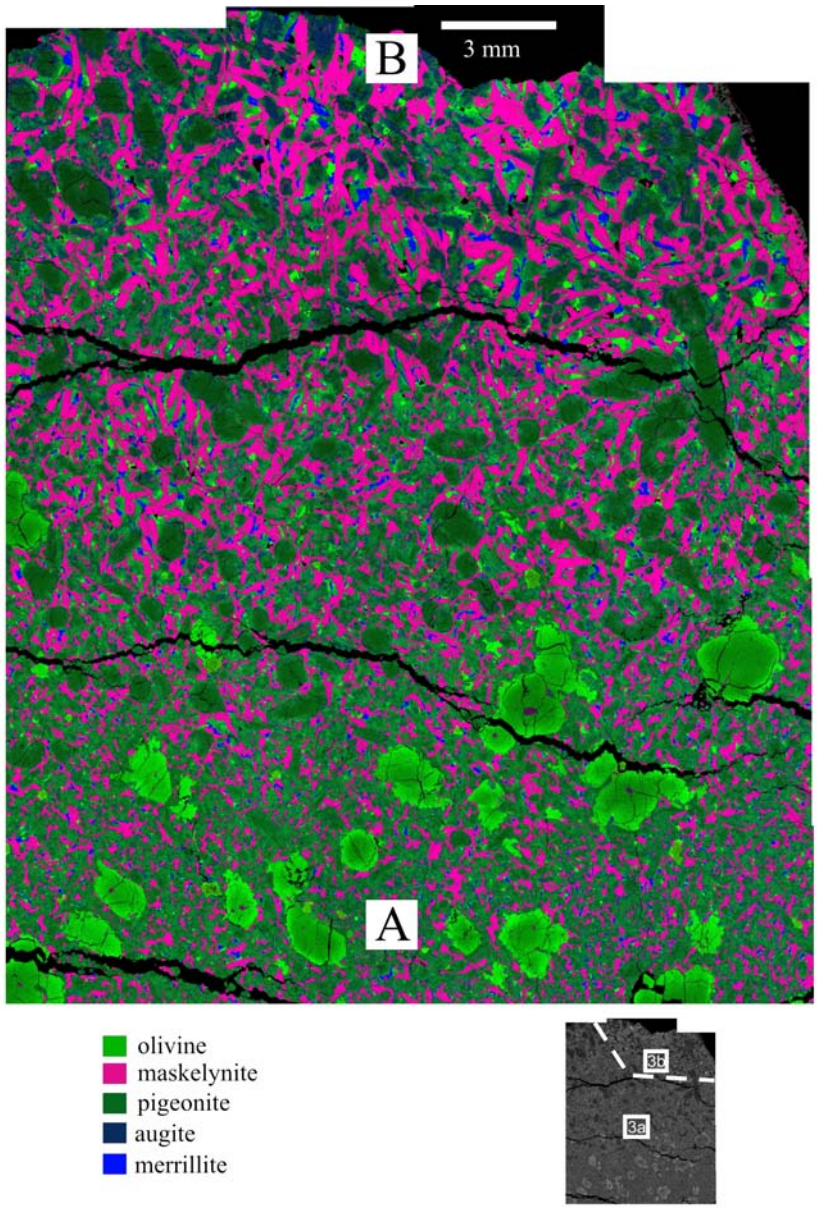

Fig. 1. Mosaic of combined Al-Fe-Ca X-ray maps (red = Al; green = Fe; blue = Ca) of a portion of section ,94, illustrating the contact between lithologies A and B (as labeled). It is important to note that olivine is restricted to lithology A, and that the small, bright green crystals in lithology B are ulvöspinel, chromite, and ilmenite. The white squares on the small grayscale figure are locations for Figs. 3a and 3b, and the dashed line within lithology B separates more primitive pigeonite phenocrysts from more evolved pyroxene assemblages similar to those in QUE 94201 (see text for discussion).

Despite a large number of studies of EETA79001 (see Meyer 2003), the contact between the two lithologies remains poorly characterized. The most detailed work to date is that of McSween and Jarosewich (1983), in which they note that the contact appears to be gradational. In this paper we examined the variation in grain size, mineral modal abundances, and mineral compositions (particularly pyroxene zonation patterns) across the contact, in order to determine the relationship between lithology A and lithology B. Based on our results, we propose a petrogenetic model in which both lithologies formed from a single cooling magma body.

ANALYTICAL TECHNIQUES

Three polished thin sections (...,94; ...,440; ...,367) of EETA79001 were studied. Sections ,94 and ,367 include both lithologies A and B, while section ,440 samples lithology B only. Of the three sections, section ,440 samples lithology B furthest from the contact.

X-ray elemental mapping for Ca, Al, Fe, Si, Mg, Cr, and Na was conducted on a Cameca SX-50 electron microprobe at 5 μm/pixel, using 4 spectrometers, an accelerating potential of 15 kV, and a beam current of 100 nA. These X-ray maps

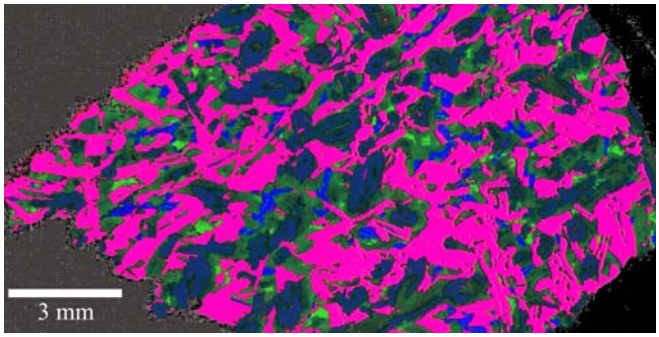

Fig. 2. Mosaic of combined Al-Fe-Ca X-ray maps (red = Al, green = Fe, blue = Ca) of section ,440 (consisting of lithology B only), indicating coarser grain size in lithology B furthest away from the contact, compared to lithology B close to the contact in Fig. 1 (thin section ,440 samples lithology B furthest away from the contact of any of the other sections). The legend is the same as for Fig. 1.

were stacked as channels, using Multispec software (Biehl and Landgrebe 2002). Modal abundances were determined from the combined stacked maps (5120 μm by 5120 μm in size) using the technique of Van Niekerk (2003). The Minimum Euclidean Distance algorithm was used during the classification process. The main error associated with this technique is the possible misclassification of pixels, which in the present study occurs mainly in the identification of different pigeonite types (i.e., magnesian versus ferroan). This error was addressed by calculations to re-assign these misidentified pixels while keeping the pigeonite totals constant, assuming that the error in pixel assignment was constant across a whole map.

Quantitative analyses were obtained on the Cameca SX-50 electron microprobe using 15 kV accelerating potential and a beam current of 20–30 nA. Counting times for Na and K were 10 s for both peak and background. Counting times for all other elements were 30 s for both peak and background. PAP procedures were used to correct matrix effects.

RESULTS

X-Ray Mapping

X-ray maps were combined in various ways to highlight chemical or textural differences between various phases. The combination Al-Fe-Ca best illustrates the contrast between the two lithologies and the nature of the contact (Figs. 1 and 2). However, we found that the combination Fe-Si-Ca (e.g., Fig. 3) allowed us better to distinguish between the different clinopyroxenes (magnesian pigeonite, ferroan pigeonite, augite), which was necessary for determination of modal abundances.

Figure 1 shows that lithology A is olivine-phyric, with phenocrysts and glomerocrysts of olivine, whereas lithology B is basaltic with no olivine. The contact between the two lithologies is nonbrecciated, and there is an absence of chill

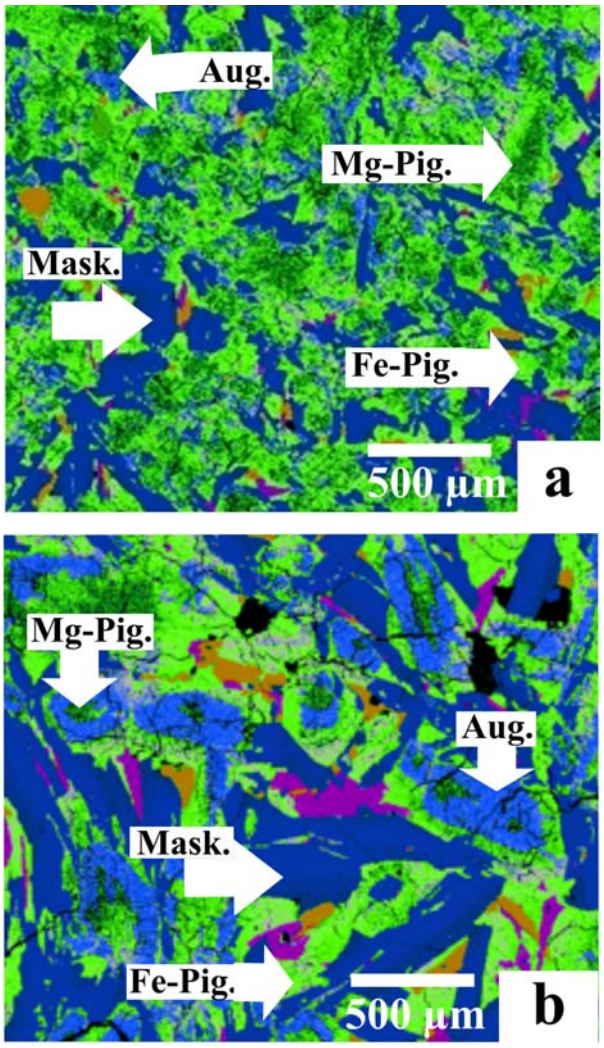

Fig. 3. Combined Fe-Si-Ca X-ray maps (red = Fe, green = Si, blue = Ca) of regions in section ,94. Mask. = maskelynite, Mg-Pig. = magnesium-rich pigeonite, Fe-Pig. = iron-rich pigeonite, Aug. = augite. The approximate locations of the regions are outlined in Fig. 1. a) Pigeonite crystals with small to nonexistent augite rims in lithology B, close to the contact (below the dashed line in Fig. 1). b) Pigeonite crystals with thicker augite rims in lithology B further away from the contact (above the dashed line in Fig. 1).

glass or any other sharply defined feature between them. Judging from Figs. 1 and 2, there is a grain size difference (best seen when looking at the maskelynite) between the two lithologies, with the groundmass of lithology A being finer-grained than lithology B. The grain size in the groundmass of lithology A appears to be uniform and does not vary with distance from the contact, whereas lithology B appears to coarsen away from the contact. Large magnesian pigeonite phenocrysts (in some cases with very thin augite rims) can be seen in lithology B close to the contact (below the dashed line in Fig. 1), and there appears to be a gradation toward smaller magnesian pigeonites with progressively thicker augite rims moving away from the contact (Figs. 3a and 3b).

Table 1. Modes (vol%) of major phases in three thin sections of EETA79001.

Section 94								Section 440
Distance[a] (mm)	0–5[b]	5–10[b]	10–15[b]	15–20[b]	20–25[b]	25–30[b]	30–35[b]	(lithology B)
Maskelynite	32.0	27.3	18.4	17.4	18.7	15.6	20.0	40.0
Augite	12.9	11.3	6.0	8.9	10.2	8.3	10.5	17.4
Mg pigeonite[c]	21.1	30.3	22.6	25.9	28.7	25.0	25.4	14.1
Fe pigeonite[c]	25.6	29.0	30.5	27.1	23.2	23.6	30.0	24.7
Olivine	0.0	0.0	20.4	19.2	17.1	25.6	12.7	0.0
Remaining phases[d]	8.5	2.1	2.1	1.5	2.0	2.0	1.4	3.8
Total	100.0	100.0	100.0	100.0	100.0	100.0	100.0	100.0
Section 367								
Distance[a] (mm)	0–5[b]	5–10[b]	10–15[b]	15–20[b]	20–25[b]	25–30[b]	30–35[b]	35–40[b]
Maskelynite	32.0	34.8	28.7	20.6	22.1	15.4	20.8	20.7
Augite	23.8	20.9	9.4	10.4	10.9	7.9	12.8	9.1
Mg pigeonite[c]	16.7	15.2	39.0	25.2	32.7	26.7	27.7	25.3
Fe pigeonite[c]	23.0	25.1	19.5	33.3	29.7	28.5	25.6	25.3
Olivine	0.0	0.0	0.0	8.7	2.7	19.4	9.9	17.8
Remaining phases[d]	4.5	4.0	3.4	1.8	1.9	2.1	3.2	1.8
Total	100.0	100.0	100.0	100.0	100.0	100.0	100.0	100.0

[a]Distance approximately from thin section edge, starting in lithology B.

[b]Points counted per map = 1,048,576; area counted per map = ~26 mm^2.

[c]Mg pigeonite and Fe pigeonite refers to the pigeonites distinguished in Fig. 1, with relatively high Mg# and low Mg#, respectively. The compositional distinction between the pigeonites becomes less pronounced further away from the contact in lithology A, and thus the error associated with determining their individual modes increases.

[d]All minor phases not separately categorized during the manual classification procedure.

Modal Analysis

Digital point counting (modal analysis) was performed on all three thin sections. For section ,440 (lithology B only) we counted the entire section. For each of sections ,94 and ,367 we conducted a traverse, counting each of 7 or 8 (respectively) adjacent maps across the contact (Table 1). Results are displayed graphically in Fig. 4. Maskelynite abundances show a decrease from a maximum in lithology B to a minimum in lithology A, and the transition across the contact appears to be gradational and systematic (Fig. 4a). Although the sizes of maskelynite grains are difficult to determine due to the amalgamation of precursor plagioclase crystals during shock, the modal variation appears to correlate with variation in grain size. Both modal abundance and grain size for maskelynite are at a maximum furthest away from the contact in lithology B, and at a minimum furthest away from the contact in lithology A (Figs. 1, 2, and 4a). The ratio of pigeonite to maskelynite (Fig. 4b) increases from a minimum in lithology B to a maximum in lithology A. Again, the transition across the contact shows no deviation from the overall trend. The traverses show that there is very little variation in the proportions of magnesian to ferroan pigeonite (Fig. 4c).

Electron Microprobe Analyses of Pyroxenes

The pyroxene assemblage in lithology A consists of pigeonite and augite (plus minor orthopyroxene that is considered by most authors to be xenolithic) (Goodrich 2003 and references therein). The pigeonite is normally zoned from a magnesian, low-Wo core to a more ferroan, higher-Wo rim, while augite is interspersed as smaller grains (see also Figs. 1 and 3a). Figures 5a and 5b illustrate typical chemical profiles through lithology A pigeonites with continuous, normal zoning. Compositions of lithology A pigeonites range from 4–15% Wo (Fig. 6a); the lowest Wo pigeonites appear to be in equilibrium with the orthopyroxenes, as noted by Goodrich (2003).

In the portion of lithology B that is closest to the contact (below dashed line in Fig. 1), pigeonite phenocrysts are similar to those in lithology A, i.e., normally zoned from magnesian to ferroan compositions (Fig. 5d), and augites occur mostly as distinct grains. Further from the contact (above dashed line in Fig. 1), lithology B pyroxenes show a more complex zonation pattern. Magnesian pigeonite is rimmed by augite, which is in turn rimmed by a more ferroan pigeonite (Figs. 3b and 5c), which is similar to pyroxenes in the basaltic shergottite Queen Alexandra Range (QUE) 94201. The magnesian pigeonite and augite have the same Mg#, as is expected at liquidus equilibria (Lindsley 1983).

An unusual feature in lithology B pyroxenes is the presence of reverse zoning in some grains (Figs. 5e and 5f). These grains sometimes show an open structure (Fig. 7), which is suggestive of skeletal growth that allowed residual liquid to enter the core, and may be similar to “soda-straw” crystals described from Zagami (Treiman and Sutton 1992).

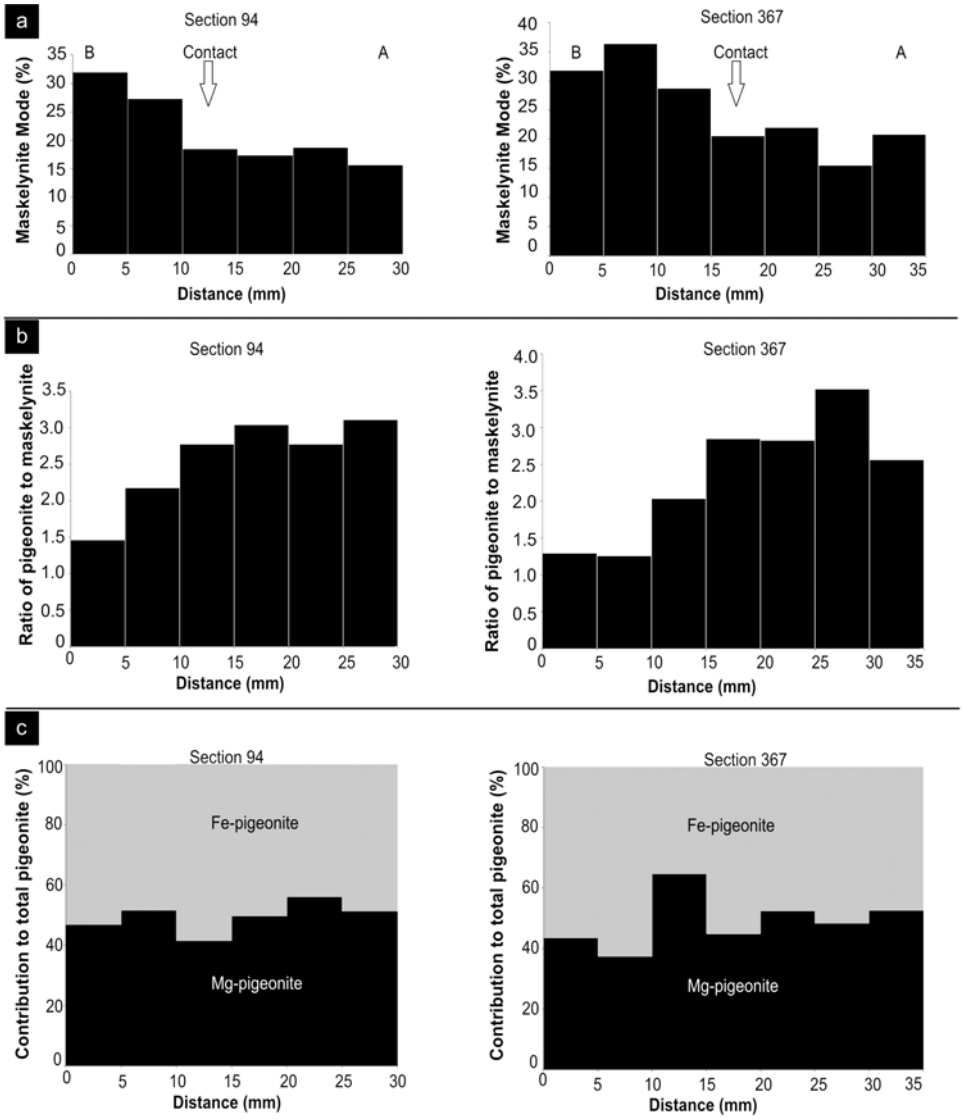

Fig. 4. Graphic display of trends produced by incremental modal analysis across the contact. Zero distance is taken to be the approximate beginning of lithology B at the edge of the thin sections. The approximate position of the contact, indicated by arrows in (a), is the same in (b) and (c). a) Variation in maskelynite content (vol%). b) Ratio of pigeonite to maskelynite. c) Variation in magnesian and ferroan pigeonite proportions.

Compositions of lithology B pigeonites range from 4–15% Wo (Fig. 6b), and augites range from 15–35% Wo. The pyroxenes in lithology B show a greater range of ferroan compositions than those in lithology A (cf. Figs. 6a and 6b).

DISCUSSION

Models for the Petrogenesis of EETA79001

McSween and Jarosewich (1983) discussed several possible models to explain the compositional and spatial relationships between lithologies A and B, including fractional crystallization of a single magma or emplacement as separate flows. Their evaluation of these models, however, was dominated by the interpretation that the megacrysts in lithology A are xenolithic (based on textural and compositional evidence for disequilibrium), which led them to focus on a mixing relationship. They calculated that the composition of the lithology A groundmass could be produced by addition (assimilation) of 10% olivine, 26% orthopyroxene, and 0.5% chromite, to a magma of lithology B bulk composition. The focus on mixing models became prevalent, though other mechanisms for the mixing were proposed. For example, Wadhwa et al. (1994) calculated that the energy needed for a lithology B-like magma to assimilate the required amount of ultramafic material in the form of solids was more than could plausibly be provided by the latent heat of crystallization, and suggested magma

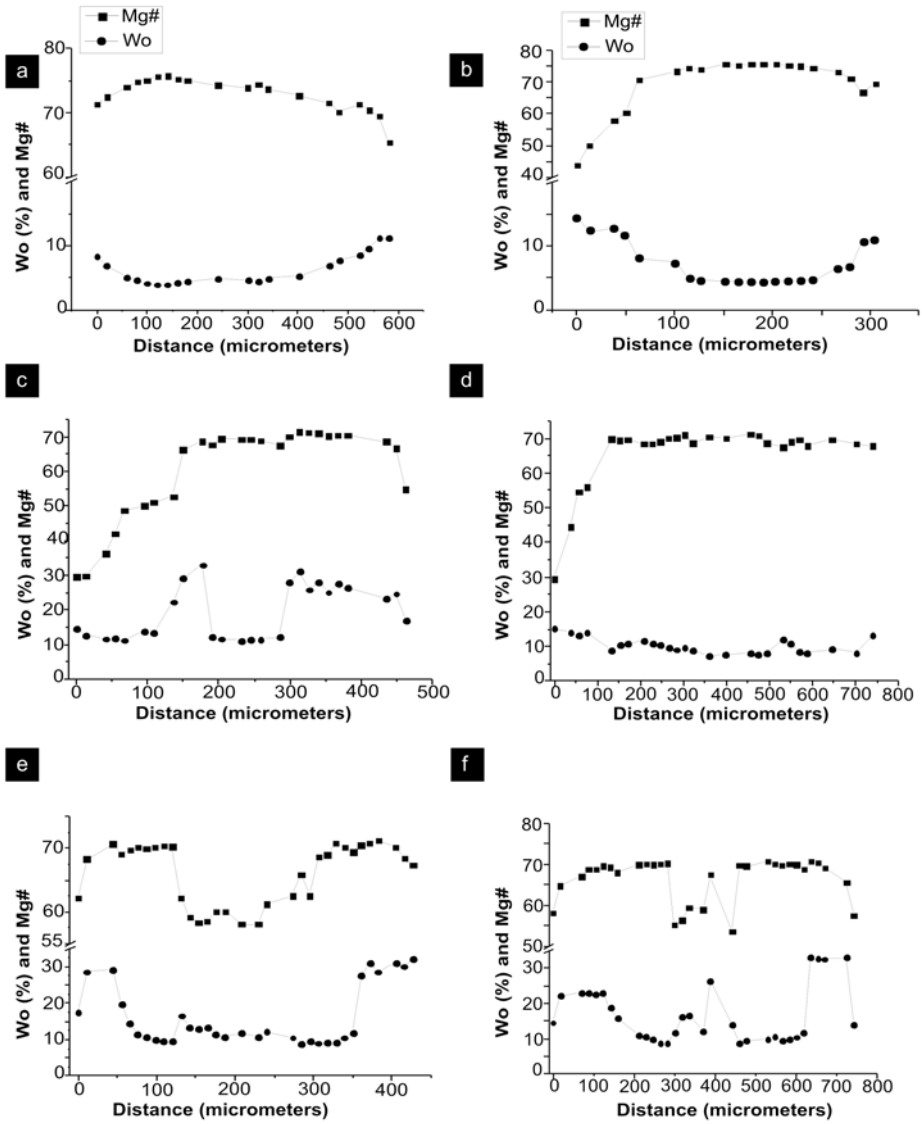

Fig. 5. Representative rim-to-rim compositional profiles through pyroxenes. Wo = wollastonite content (mol%), Mg# = magnesium number. (a) and (b) Lithology A pyroxenes. (c) and (d) Lithology B pyroxenes. (e) and (f) Lithology B reversely zoned pyroxenes (refer to text).

mixing as an alternative. However, Mittlefehldt et al. (1999) argued from trace element data that the lherzolitic endmember in any mixing model must have contained little melt and suggested that the energy for assimilation was provided by impact, though other authors (Warren et al. 1999; Neal et al. 2001) have pointed out problems with siderophile element abundances in this model.

In contrast to these mixing models, Goodrich (2003) argued that the majority of the material in lithology A formed by continuous crystallization of a single magma, with the amount of xenolithic material being minor (limited to the most magnesian olivine, plus the chromite and true orthopyroxene). This argument was based on the demonstration that 1) groundmass pigeonites are in equilibrium with most of the olivine (despite previous assertions to the contrary), and 2) the liquid represented by melt inclusions in this olivine crystallizes to a phase assemblage consistent with that observed. In addition, she disagreed with the interpretation (e.g., McSween and Jarosewich 1983) that the megacrysts exhibit textural disequilibrium with the groundmasss. We will discuss this issue further in the following section.

Textural Evidence for Assimilation and Mixing?

The textural argument that the megacrysts in lithology A are xenocrysts is based on the anhedral shapes (interpreted to result from resorption) of some of the olivine crystals, and on the observation that some olivine grains occur as glomerocrysts (with or without attached orthopyroxene and chromite). Resorption features of olivine cannot, however, automatically be attributed to disequilibrium events such as

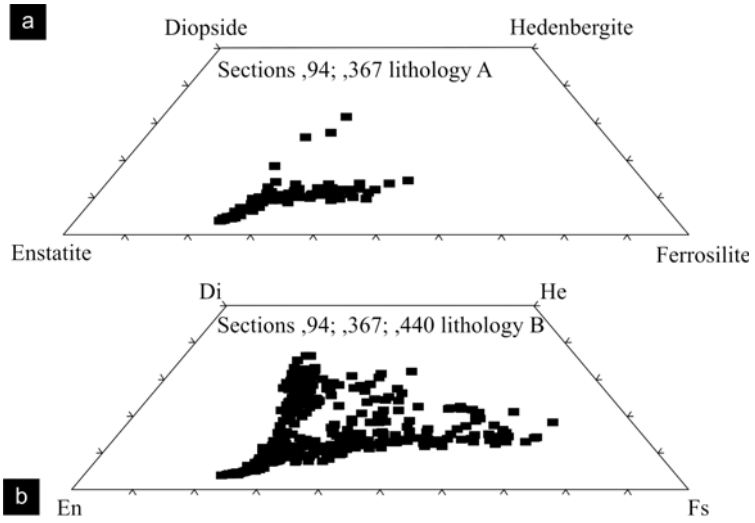

Fig. 6. a) Pyroxene compositions in lithology A. b) Pyroxene compositions in lithology B (in mol% endmembers).

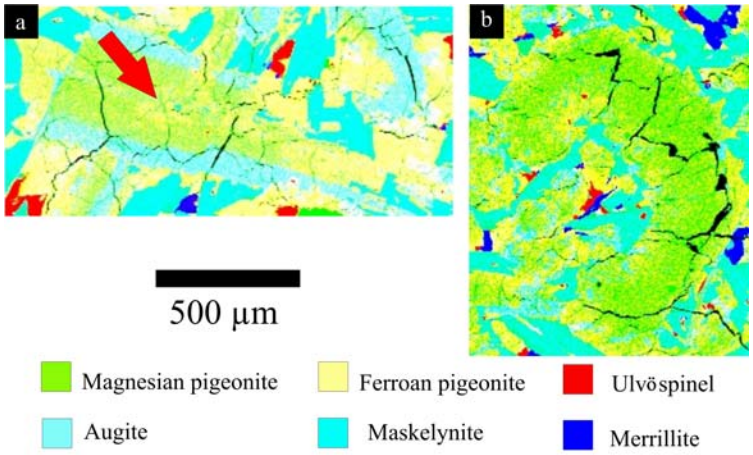

Fig. 7. a) An example of reversely zoned pyroxenes in lithology B that may be due to skeletal crystal growth. Note the presence of ferroan pigeonite in the inner part of the assemblage, indicated by the arrow. b) Skeletal pigeonite phenocryst close to the contact with lithology A, partially enclosing maskelynite, ferroan pigeonite, whitlockite, and ulvöspinel in the center of the crystal. All images are processed Fe-Si-Ca X-ray maps.

magma mixing or xenolith assimilation. Equilibrium resorption (i.e., the peritectic reaction of olivine to orthopyroxene) in tholeiitic basalts is commonly evidenced by rounded and/or embayed olivine (Cox et al. 1979; Evans and Moore 1968; McBirney 1993), and resorption can also result from remobilization of olivine from colder parts of a magma column to a hotter region (Helz 1987). Likewise, glomerocrysts (particularly of early phases expected to crystallize together) are not necessarily xenolithic fragments. They commonly form in lava flows, lava lakes, and magma chambers (Heltz 1987; Schwindinger 1999; Shelley 1993).

Thus, we conclude that there is no textural requirement for the majority of the olivine in lithology A to be xenolithic. Since there is no compositional requirement either (Goodrich 2003), this opens the door to reconsidering models that were dismissed by McSween and Jarosewich (1983), such as fractional crystallization of a single magma, or emplacement as separate flows, to explain the relationship between lithologies A and B. We first discuss the latter.

Does the Contact Represent Two Lava Flows?

Observations of lava flows in Hawai‘i reveal that a flow seldom, if ever, overlaps with concurrent flows (e.g., Gregg and Keszthelyi 2004). Pahoehoe flows chill quickly due to a thermal differential between the lava and the atmosphere, and as a result form a glassy rind at the top. Any successive lava flows overlap with such a chilled flow only after the latter has solidified or cooled considerably. Therefore a glassy chill zone can be expected to be preserved between the top contact of a basalt and the bottom contact of an overlying one. The study of Burkhard (2003) showed that a flow that has not

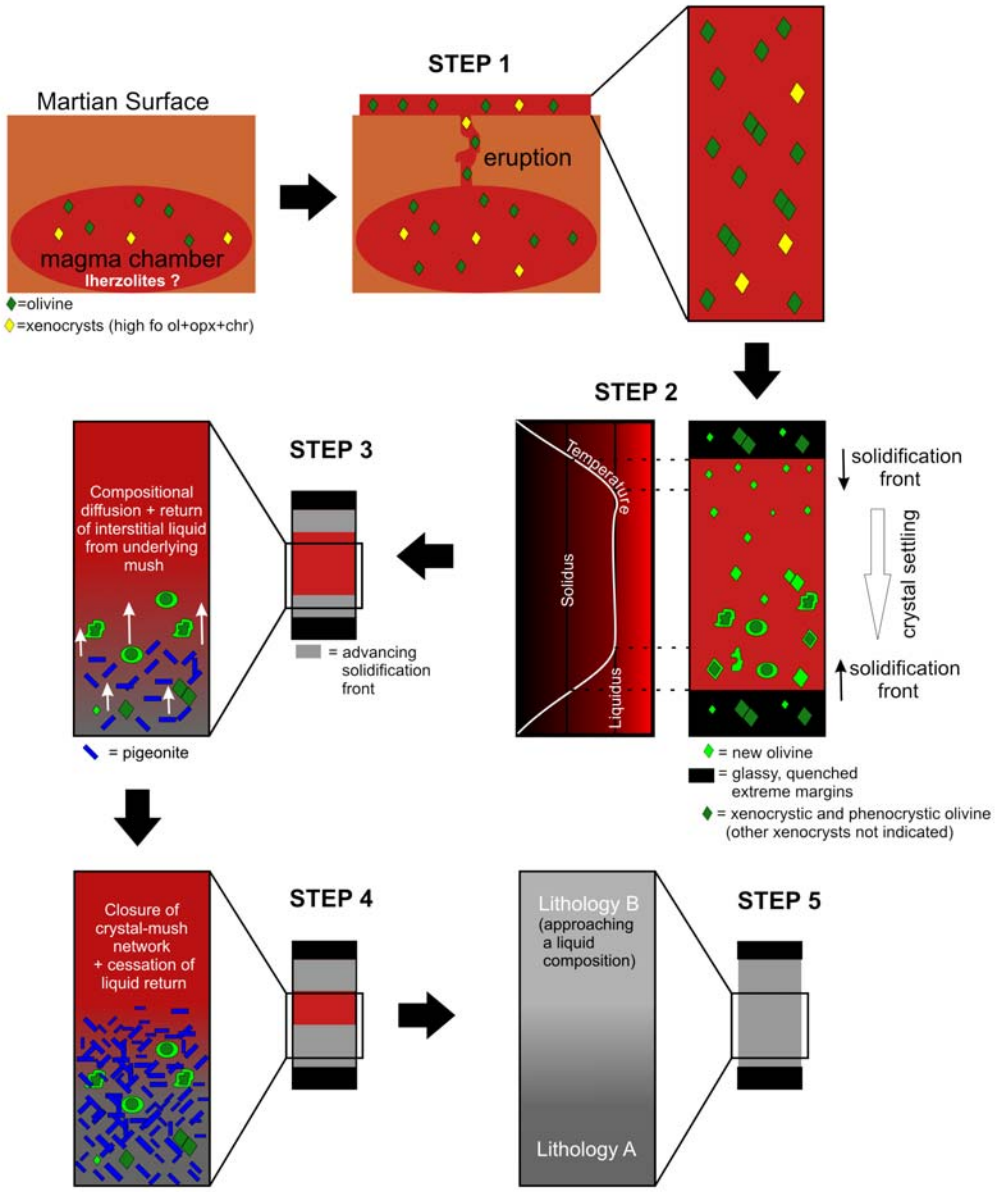

Fig. 8. Schematic demonstration (simplified and not to scale) of the temporal evolution of a magma column leading to the development of lithologies A and B with a gradational contact (see text for a detailed description). Ol = olivine, opx = orthopyroxene, chr = chromite.

solidified completely may experience reheating at its upper contact when a second flow is emplaced on top of it. For recrystallization of the glassy chill zone to take place during reheating, and to allow for the growth of plagioclase, the chilled solid has to be reheated to a minimum temperature of 920 °C. For the Hawai'ian basalts studied, it was calculated that the basal flow must have been above 700 °C at the time that the top flow, with a known temperature of 1160 °C, was emplaced. The top basalt shows increasing grain size with depth, which is consistent with faster cooling at its top and slower cooling at its base due to the thermal gradient that develops during radiation of heat to the atmosphere. The basal basalt, which would be expected to show the same gradation in grain size as a result of its original cooling history, does not, and is holocrystalline at its top with an absence of chill glass. The inference, therefore, is that reheating of the basal flow's chill zone by the overlying flow induced recrystallization. It should be noted, however, that the style of lava emplacement in the Burkhard (2003) study is rare, and is only observed when the lobes are from the same lava flow.

By analogy to the Hawaiian lava flows described above, the absence of chill glass at the contact in EETA79001 implies that the two lithologies can represent two separate lava flows only if one was emplaced while the other still retained significant heat, so that the original chill zone on the first flow experienced reheating and recrystallization. If

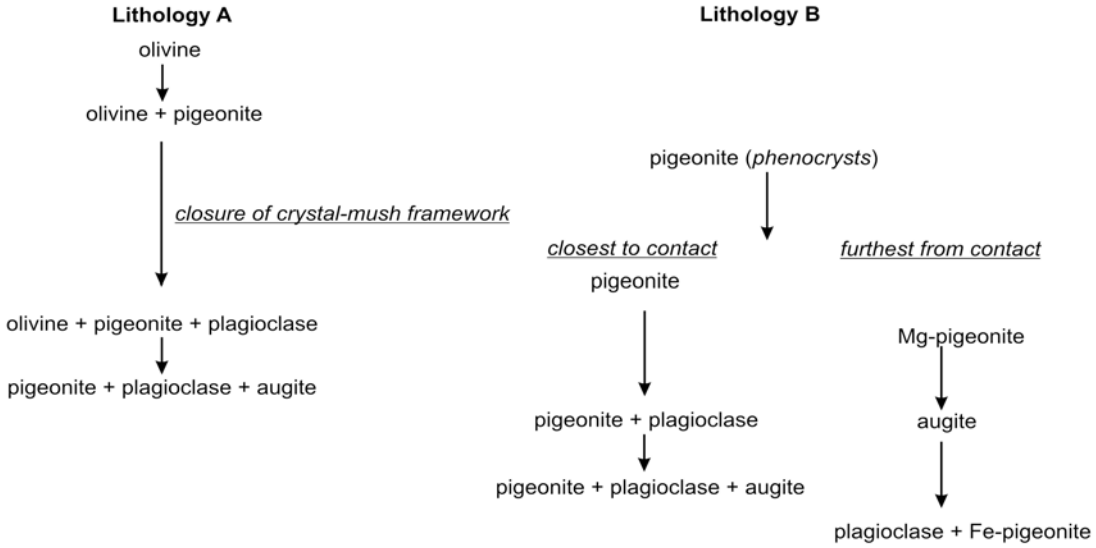

Fig. 9. Crystallization sequences of major phases in lithologies A and B as a result of the processes described in our model (see text). The derivation of the sequence for lithology A has been described in detail in Goodrich (2003).

lithology B represented a thin lava flow emplaced on top of lithology A, then we would expect it to show a decrease in grain size away from the contact. If it represented a thick flow, then we would expect uniform grain size away from the contact. Neither is the case. There is an increase in grain size in lithology B moving away from the contact. Therefore, lithology B cannot represent a flow emplaced on top of lithology A with contemporaneous reheating of a chilled margin. Furthermore, the presence of magnesian pigeonite phenocrysts concentrated in lithology B near the contact makes it unlikely that lithology A represents a flow emplaced on top of lithology B, since reheating of a chill zone is unlikely to have produced these. Thus, we conclude that lithologies A and B of EETA79001 are unlikely to represent two separate flows.

Fractionation Model for the Petrogenesis of EETA79001

Fractionation of magmas in magma chambers, dikes, sills, lava lakes, and lava flows is a well-documented process in igneous environments. In the following section, we propose a model in which crystal settling, in situ crystallization (as described by Langmuir 1989), and crystal-mush compaction are responsible for continuous differentiation in a lava flow. We also demonstrate that this model (summarized in Fig. 8) can account for the gradational nature of the contact of EETA79001, as well as many of its other characteristics.

Stratigraphic Evolution

Step 1: The first step of this model involves the eruption of a basaltic magma carrying phenocrysts and glomerocrysts of olivine crystallized in a magma chamber, as well as minor amounts (Goodrich 2003) of xenocrystic olivine, orthopyroxene, and chromite.

Step 2: Conduction of heat induces concurrent downward and upward solidification of magma at the top and base of the flow, respectively (while the insulated interior remains above its liquidus). This leads to formation of crystal-mush zones at the solidification fronts. Crystal settling of the erupted solids occurs, coupled with crystallization of a new generation of olivine in equilibrium with the surface environment. The new olivine is represented by the more fayalitic overgrowth on pre-eruptive olivine and also as new crystals lacking more forsteritic cores. In some cases, the pre-eruptive crystals settling from the top part of the magma column will stick to newly formed crystals in the lower part of the flow, producing glomerocrysts of inhomogeneous olivines. Olivine settling of this kind has been observed in Hawaiian lava lakes and flows, and is also expected to occur in magma chambers (Heltz 1980; Heltz 1987; Moore and Evans 1967; Rowland and Walker 1988; Schwindinger 1999; Shelley 1993). Furthermore, the upper and lower quenched crusts may entrap some of the early phenocrysts.

Step 3: Crystal settling will deplete the upper part and enrich the lower part of the flow in phenocrysts (both pre-eruptive and post-eruptive), and in this case must have proceeded to the extreme of forming an olivine-free zone (e.g., Rowland and Walker 1988). As fractionation proceeds due to crystal settling, a vertical chemical gradient is established. This gradient is ultimately responsible for the differences between the lithology A groundmass and lithology B.

After olivine, pigeonite will be the dominant phase crystallizing (up to ~65% crystallization) (Goodrich 2003) in

the lower crystal-mush solidification front. This leads to the onset of in situ crystallization (as described by Langmuir 1989), which expels residual liquid from the solidification zone into the overlying liquid. Elements that are incompatible in pigeonite will be transferred from the solidification zone to the overlying (to become lithology B) melt. This diffusion process becomes more pronounced as crystallization proceeds, whereas processes like mixing in the solidification zone (lithology A melt) becomes progressively more restricted. At 25–50% pigeonite crystallization, development of crystal frameworks (Jerram et al. 2003; Philpotts et al. 1996, 1998) may also contribute significantly to injection of residual liquid into the hot overlying liquid.

The overlying hot liquid will eventually cool to the pigeonite liquidus and remain there long enough to form some phenocrysts which accumulate near the contact with the solidification zone. At this point, the pigeonite crystal-mush in lithology A has strengthened sufficiently that the phenocrysts from the overlying melt cannot mix extensively with the picritic zone. Some limited intermingling of crystals (i.e., pigeonite phenocrysts from lithology B and a few olivine phenocrysts from lithology A) occurs, however, at the contact with the solidification front (this zone may be the material recognized by Mittlefehldt and Lindstrom [1999] as lithology AB).

Step 4: The insulated interior of the flow will now continue to move down its liquidus in accordance with the thermal gradient. Crystallization will advance progressively upward from the base of the lithology B melt. The chemical gradients (described in the Crystallization Chemistry section) that accompany this progressive crystallization lead to plagioclase crystallizing progressively earlier. Therefore, the progressive grain size increase from lithology A groundmass into and throughout lithology B may result from more and more space being available to plagioclase as it crystallizes. By this time, the crystal-mush framework at the contact with lithology A would have sealed off (at 50–60% solid) so that interstitial liquid could no longer be expelled. Subsequently, minor phases crystallize from the small remaining pockets of interstitial liquid.

Step 5: When the bulk of lithology B (i.e., far from the pigeonite phenocryst accumulation zone near the contact) finally crystallizes, its composition approximates that of a liquid because the melt that it represents has crystallized in the interior of the lava flow where it was trapped between the upper and lower solidification fronts (i.e., it was a closed system). Thus, the similarity of its pyroxenes to those in QUE 94201 (shown to closely approximate a liquid composition) (McKay et al. 2002) is not surprising. Our model shows, however, that this liquid did not exist as a distinct lava flow, but rather is a partial fractionate of a parental melt, cumulatively represented by both lithologies A and B (and whatever is missing of the stratigraphy).

Crystallization Chemistry

Figure 9 illustrates the crystallization sequence of the major phases in lithologies A and B. Note that there is a continuous temporal offset between solidification of vertically adjoining portions of the magma column, as well as continuous chemical changes in the melt due to the process of in situ crystallization. This is probably more pronounced for lithology B, which is located very close to the absolute center of the two advancing solidification fronts, than for lithology A, which is located closer to the margins of the flow. Therefore the effect of chemical variation will possibly be more pronounced on a smaller scale in lithology B.

Since pigeonite is the dominant phase on the liquidus in lithology A and the dominant phase crystallizing at the time of closure of the crystal-mush framework (at >50% solids), Mg and Fe should be enriched in lithology A while elements that are less compatible in pigeonite (particularly Ca) are enriched in lithology B (the expelled residual liquid). The bulk compositions (McSween and Jarosewich 1983) of the two lithologies are consistent with this.

The dominance of Mg and Fe and relative depletion of Ca in lithology A lead to continuous pigeonite zonation from magnesian to ferroan compositions, with augite appearing only as a minor phase at ~80% crystallization. As the crystal-mush framework of lithology A strengthens and the solidification front progresses into the lithology B portion of the magma column, Mg-pigeonite phenocrysts will begin to grow in a zone close to the contact (i.e., below the dashed line in Fig. 1), after which pigeonite will continue to crystallize progressively higher up in the magma column.

The Ca gradient throughout the magma column will affect an incrementally earlier crystallization (ranging for example from entry at ~80% to ~60% crystallization) of augite (and also plagioclase), moving into and through lithology B. The relative enrichment of Ca over Fe furthest from the contact in lithology B will cause augite to crystallize before ferroan pigeonite (fractional crystallization modeling shows entry at ~60% crystallization) at Mg# similar to that of the magnesian pigeonite it rims. Furthermore, this Ca gradient accounts for the progressively thicker augite rims and smaller magnesian pigeonite cores moving into lithology B. The ferroan pigeonite outer rims on the pyroxenes are formed after the appearance of plagioclase (at a relatively evolved stage when Fe is significantly enriched) starts to once again deplete Ca.

Strontium Isotopes

Existing strontium (Sr) isotopic data (Nyquist et al. 1986; Nyquist et al. 2001b; Wooden et al. 1982) for lithologies A and B suggest the possibility that the two lithologies have different initial ($^{87}Sr/^{86}Sr$) ratios (lithology A < lithology B), which might preclude their being products of the same magma. At present, however, the exact constraints provided by these data are unclear. Wooden et al. (1982) and

Nyquist et al. (1986) document isotopic heterogeneity of uncertain origin within, and between, lithologies A, B, and C (impact glass). For example, lithology A whole rock compositions do not plot on the lithology A mineral isochron. Nyquist et al. (1986) suggest that the mineral isochron may be lower than the whole rock average because the mineral separates were coarse, and incorporated a xenocryst component. If this were true, a xenocryst-free isochron would place the initial ($^{87}Sr/^{86}Sr$) values of the two lithologies much closer to each other. Furthermore, the impact glasses (lithology C) have a range of initial ($^{87}Sr/^{86}Sr$) compositions encompassing those of both lithology A and B (and even some outside the range), which indicates that the post-crystallization environment has not remained closed. Finally, redetermined initial ($^{87}Sr/^{86}Sr$) values for lithology B (Nyquist et al. 2001b), which yield an age within error of that of lithology A, differ significantly from the original value (Nyquist et al. 1986), which suggests that Sr(I) ratios may be heterogeneous within lithology B itself. Nyquist et al. (2001b) point out that there is variation of initial ($^{87}Sr/^{86}Sr$) among subsamples of shergottites as well as nakhlites. The cause of this variation is unknown and might require unusual petrogenetic processes (Nyquist et al. 2001a), although Nyquist et al. (2006) speculate that heterogeneity in Zagami due to variation of inherited pyroxene cores offer an explanation for variation in other shergottites as well.

CONCLUSIONS

1. Results from a study of grain size, mineral modal abundances, and mineral compositional patterns across the contact between lithology A and lithology B of EETA79001 show that the contact is gradational. We suggest that it could be a primary igneous feature consistent with crystallization of a single cooling magma body. We present a model that produces lithologies A and B through olivine crystal settling and in situ fractionation (Langmuir 1989) in such a magma.
2. This model implies that EETA79001 represents a partial record of an igneous differentiation event in the Martian crust, and establishes a direct connection between olivine-phyric and basaltic shergottites (though the connection need not extend to all shergottites). Furthermore, it suggests that shergottite (even basaltic) parent magmas may be represented by compositions similar to that preserved in melt inclusions in olivine in lithology A (Goodrich 2003).
3. It remains to be determined whether this model is consistent with Sr isotopic and other age data for EETA79001. Microanalytical isotopic analyses across the contact may reveal whether the observed gradational change in textural and compositional features is accompanied by a gradational or sharp (or no) isotopic boundary.

Acknowledgments–Dr. Treiman is thanked for editorial duties, and Drs. Jerram, Mittlefehldt, Misawa, and Harvey are thanked for their reviews of the manuscript. This work was supported in part by NASA grants NAG 5-11591 to Klaus Keil and NNG05GH72G to Cyrena Goodrich. This is Hawai‘i Institute of Geophysics and Planetology publication no. 1488 and School of Ocean and Earth Science and Technology publication no. 7121.

Editorial Handling—Dr. Allan Treiman

REFERENCES

Biehl L. and Landgrebe D. 2002. Multispec-a tool for multispectral-hyperspectral image data analysis. *Computers & Geosciences* 28: 1153–1159.

Burkhard D. J. M. 2003. Thermal interaction between lava lobes. *Bulletin of Volcanology* 65:136–143.

Cox K. G., Bell J. D., and Pankhurst R. J. 1979. *The interpretation of igneous rocks*. London: George Allen & Unwin Ltd. 450 p.

Evans B. W. and Moore J. G. 1968. Mineralogy as a function of depth in the prehistoric Makaopuhi tholeiitic lava lake, Hawai‘i. *Contributions to Mineralogy & Petrology* 17:85–115.

Goodrich C. A. 2002. Olivine-phyric Martian basalts: A new type shergottite. *Meteoritics & Planetary Science* 37:B31–B34.

Goodrich C. A. 2003. Petrogenesis of olivine-phyric shergottites Sayh al Uhaymir 005 and Elephant Moraine A79001 lithology A. *Geochimica et Cosmochimica Acta* 67:3735–3772.

Gregg K. P. and Keszthelyi L. P. 2004. The emplacement of pahoehoe toes: Field observations and comparison to laboratory simulations. *Bulletin of Volcanology* 66:381–391.

Heltz R. T. 1980. Crystallization history of Kilauea Iki lava lake as seen in drill core recovered in 1967–1979. *Bulletin of Volcanology* 43:675–701.

Heltz R. T. 1987. Diverse olivine types in lava of the 1959 eruption of the Kilauea volcano and their bearing on eruption dynamics. In *Volcanism in Hawai‘i*, edited by Decker R. W. Wright T. L., and Stauffer P. H. U.S. Geological Survey Professional Paper #1350. Washington, D.C.: U.S. Government Printing Office. pp. 691–722.

Jerram D. A., Cheadle M. J., and Philpotts A. R. 2003. Quantifying the building blocks of igneous rocks: Are clustered crystal frameworks the foundation? *Journal of Petrology* 44:2033–2051.

Langmuir C. H. 1989. Geochemical consequences of in situ crystallization. *Nature* 340:199–205.

McBirney A. R. 1993. *Igneous petrology.* Boston: Jones and Bartlett. 508 p.

McKay G., Koizumi E., Mikouchi T., and Lee L. 2002. Crystallization of shergottite QUE 94201: An experimental study (abstract #2051). 33rd Lunar and Planetary Conference. CD-ROM.

McSween H. Y. Jr. and Jarosewich E. 1983. Petrogenesis of the Elephant Moraine A79001 meteorite: Multiple magma pulses on the shergottite parent body. *Geochimica et Cosmochimica Acta* 47:1501–1513.

McSween H. Y. Jr. and Treiman A. H. 1998. Martian meteorites. In *Planetary materials*, edited by Papike J. J. Reviews in Mineralogy, vol. 36. Washington, D.C., Mineralogical Society of America. pp. 6-1–6-53.

Meyer C. 2003. EETA79001. Mars meteorite compendium. Houston, Texas: NASA. JSC #27672 Revision C. http://

curator.jsc.nasa.gov/antmet/mmc/index.cfm. Last accessed 2007.

Mittlefehldt D., Lindstrom D. J., Lindstrom M. M., and Martinez R. R. 1999. An impact-melt origin for lithology A of Martian meteorite Elephant Moraine A79001. *Meteoritics & Planetary Science* 34:357–367.

Mittlefehldt D. and Lindstrom M. M. 1999. Petrology and geochemistry of Martian meteorites EETA79001 and ALHA77005 (abstract #1817). 30th Lunar and Planetary Science Conference. CD-ROM.

Moore J. G. and Evans B. W. 1967. The role of olivine in the crystallization of the prehistoric Makaopuhi tholeiitic lava lake, Hawai'i. *Contributions to Mineralogy and Petrology* 15:202–223.

Neal C. R., Ely J. C., and Jain J. C. 2001. New platinum group element (PGE) data for Martian meteorites: The influence of igneous processing (abstract #1682). 32nd Lunar and Planetary Conference. CD-ROM.

Nyquist L. E., Wiesman H., Shih C. Y., and Bansal B. 1986. Sr isotopic systematics of EETA79001 glass (abstract). 17th Lunar and Planetary Conference. pp. 624–625.

Nyquist L., Bogard D. D., Shih C.-Y., Greshake A., Stöffler D., and Eugster O. 2001a. Ages and geologic histories of Martian meteorites. *Space Science Reviews* 96:105–164.

Nyquist L. E., Reese Y., Wiesman H., and Shih C. Y. 2001b. Age of EET79001B and implications for shergottite origins (abstract #1407). 32nd Lunar and Planetary Conference. CD-ROM.

Nyquist L. E., Shih C. Y., and Reese Y. D. 2006. Initial isotopic heterogeneities in Zagami: Evidence of a complex magmatic history (abstract #5143). *Meteoritics & Planetary Science* 41: A135.

Philpotts A. R., Carrol M., and Hill J. M. 1996. Crystal-mush compaction and the origin of pegmatite segregation sheets in a thick flood-basalt flow in the Mesozoic Hartford Basin, Connecticut. *Journal of Petrology* 37:811–836.

Philpotts A. R., Shi J., and Brustman C. 1998. Role of plagioclase crystal chains in the differentiation of partly crystallized basaltic magma. *Nature* 395:343–346.

Rowland S. K. and Walker G. P. L. 1988. Mafic-crystal distributions, viscosities, and lava structures of some Hawai'ian lava flows. *Journal of Volcanology & Geothermal Research* 35:55–66.

Schwindinger K. R. 1999. Particle dynamics and aggregation of crystals in a magma chamber with application to Kilauea Iki olivines. *Journal of Volcanology & Geothermal Research* 88: 209–238.

Shelley D. 1993. *Igneous and metamorphic rocks under the microscope*. London: Chapman & Hall. 445 p.

Treiman A. H. and Sutton S. R. 1992. Petrogenesis of the Zagami meteorite: Inferences from synchrotron X-ray (SXRF) microprobe and electron microprobe analyses of pyroxenes. *Geochimica et Cosmochimica Acta* 56:4059–4074.

Treiman A. H., Gleason J. D., and Bogard D. D. 2000. The SNC meteorites are from Mars. *Planetary and Space Science* 48: 1213–1230.

Van Niekerk D. 2003. Modal analysis and phase identification in meteorite thin sections using "freeware" for PC. (abstract #2015). 34th Lunar and Planetary Science Conference. CD-ROM.

Wadhwa M., McSween H. Y. Jr. and Crozaz G. 1994. Petrogenesis of shergottite meteorites inferred from minor and trace element microdistributions. *Geochimica et Cosmochimica Acta* 58:4213–4229.

Warren P. H., Kallemeyn G. W., and Kyte F. T. 1999. Origin of planetary cores: Evidence from highly siderophile elements in Martian meteorites. *Geochimica et Cosmochimica Acta* 63: 2105–2122.

Wooden J., Shih C.-Y., Nyquist L., Bansal B., Wiesmann H., and McKay G. 1982. Rb-Sr and Sm-Nd isotopic constraints on the origin of EETA79001: A second Antarctic shergottite (abstract). 13th Lunar and Planetary Conference. pp. 879–880.